

# High-speed Atomic Force Microscopy for Capturing Dynamic Behavior of Protein Molecules at Work\*

Toshio Ando<sup>†</sup>

*Department of Physics, Graduate School of Science and Technology,  
Kanazawa University, Kakuma-machi, Kanazawa 920-1192, Japan, and CREST/JST*

Noriyuki Kodera

*Department of Physics, Graduate School of Science and Technology,  
Kanazawa University, Kakuma-machi, Kanazawa 920-1192, Japan,*

Takayuki Uchihashi

*Department of Physics, Graduate School of Science and Technology,  
Kanazawa University, Kakuma-machi, Kanazawa 920-1192, Japan, and CREST/JST,*

Atsushi Miyagi, Ryo Nakakita, Hayato Yamashita, and Keiko Matada

*Department of Physics, Graduate School of Science and Technology,  
Kanazawa University, Kakuma-machi, Kanazawa 920-1192, Japan*

(Received 7 October 2005; Accepted 17 November 2005; Published 7 December 2005)

It seems that only the atomic force microscope (AFM) has a potential to trace a protein in action with high spatial and temporal resolution. To realize that potential, we have been developing a high-speed AFM. We have made efforts not only to enhance the scan speed but also to reduce the tip-sample interaction force as much as possible. The high-speed AFM can capture moving protein molecules and weakly interacting protein molecules on video without disturbing their physiological function. Here we review our studies carried out over the past 10 years, and our preliminary work toward the next generation of the instrument. [DOI: 10.1380/ejsnt.2005.384]

Keywords: Atomic force microscopy; biological aspects of nanostructures; proteins

## I. INTRODUCTION

When protein is functioning in solution, its structure is dynamically changing. The structural dynamics must be tightly associated with the mechanism by which the protein produces its physiological function. It is, therefore, desirable to visualize directly the dynamic behavior of individual protein molecules in action; however, the technology for direct visualization is lacking. Thus, we have to infer their dynamic behavior from various indirect observations, which can be misleading.

The atomic force microscope (AFM) has now become an indispensable tool for imaging and characterizing surface nanostructures in various environments. However, many users of AFM have found that capturing a single image takes a long time. Because AFM relies on mechanical scanning of the sample stage or the cantilever, it is difficult to enhance the scan speed without producing mechanical noises. The limited imaging rate not only imposes on AFM users' patience but also restricts the scope of examinable dynamics of the sample. This restriction has discouraged biologists from studying dynamic processes of biological macromolecules using AFM, although the capability of AFM to view a nanometer-scaled world in an aqueous environment was a very welcome addition to biological studies.

The tapping mode of the AFM operation [1] is most

suitable for soft and fragile samples; the vertically oscillating cantilever tip taps the sample surface intermittently, so that lateral force exerted between the tip and the sample can be minimized. During a raster scan of the sample stage in the horizontal plane, the cantilever's oscillation amplitude (and hence the tapping force) is kept constant by moving the sample stage up or down, depending on the sample height. This feedback operation is indispensable to avoid strong tip-sample interaction. Therefore, the scan speed (and hence the imaging rate) is determined not only by the scanner's bandwidth, in which it can operate without producing mechanical noises, but also by the feedback bandwidth. Almost all AFM devices are involved in the feedback loop and therefore have to be optimized for the high-speed feedback operation.

Efforts to achieve a high imaging rate with AFM have been, as far as we know, initiated by three groups; Paul Hansma's lab at UCSB, Calvin Quate's lab at Stanford Univ., and our group at Kanazawa Univ. The UCSB group developed small cantilevers with a high resonant frequency to increase their response speed [2], in addition to an optical lever system compatible with the small cantilevers [3]. The Stanford group developed self-actuating/sensing cantilevers [4] to overcome the slow z-scan rate of the conventional tube scanner, and cantilever arrays [5] to image a large area at once. However, these efforts alone could not lead to a high imaging rate because other devices remained to be developed. Prior to 2001, we developed various devices, including a high-speed stage scanner, small cantilevers, an optical lever system for the small cantilevers, and a fast amplitude-to-DC converter that can output the amplitude signals at every half cycle of the cantilever oscillation. By assembling these devices, we made the first generation of high-speed AFM

\*This paper was presented at International Symposium on Surface Science and Nanotechnology (ISSS-4), Saitama, Japan, 14-17 November, 2005.

<sup>†</sup>Corresponding author: [tando@kenroku.kanazawa-u.ac.jp](mailto:tando@kenroku.kanazawa-u.ac.jp)

that could capture moving protein molecules on video at 80 ms/frame [6, 7]. However, it became clear later that the tip-sample interaction force was not small enough to image fragile samples or weakly interacting proteins [8]. To overcome this serious problem we further developed various devices and techniques [8, 9]. Now the second generation of our high-speed AFM can capture weakly interacting proteins without disturbing their physiological action. In this article, we review our efforts made in the past decade to achieve a high imaging rate ( $\sim 50$  ms/frame) as well as our challenges as we move to the next generation of AFM technology.

## II. THEORETICAL CONSIDERATIONS

Sulcheck qualitatively analyzed how the feedback bandwidth in the tapping mode is affected by various factors, such as the set-point, the sample height, and the resonant frequency and oscillation amplitude of the cantilever [10]. From the qualitative description, we cannot get a prospect of how extensively we have to improve various devices in order to enhance the feedback bandwidth. Here we find a semi-quantitative description.

Suppose that a sample on a substrate has a periodicity of  $\lambda$  and that the sample stage is moved horizontally with a velocity of  $V_s$ , the spatial frequency of  $1/\lambda$  is converted to a temporal frequency of  $f \equiv V_s/\lambda$ . This is the feedback frequency with which the sample stage is moved in the  $z$ -direction. The most rigid definition of the feedback bandwidth is the feedback frequency at which the feedback operation is phase-delayed less than  $45^\circ$ . This corresponds to a time delay of  $1/8f$ . The feedback loop contains various delaying steps. One of the main delays is the time required for reading the cantilever's oscillation amplitude. It takes at least a time between  $1/f_c$  and  $1/2f_c$ , where  $f_c$  is the cantilever's resonant frequency. When the cantilever's amplitude changes only at the bottom of swing (where its tip taps the sample surface), it takes  $1/f_c$ , while it takes  $1/2f_c$  when the amplitude changes at both the bottom and peak of swing (this occurs with cantilever oscillation with a large quality factor,  $Q_c$ ). In solution, the cantilever's amplitude changes solely at the bottom of swing due to a large viscous drag force. The other main delays are the cantilever's response time ( $Q_c/\pi f_c$ ), and (3) the  $z$ -scanner's response time ( $Q_s/\pi f_s$ ), where  $Q_s$  and  $f_s$  are the quality factor and the resonant frequency of the  $z$ -scanner, respectively. These delays and additional delays (the total,  $\Delta$ ) give the following relationship.

$$f < \frac{f_c/8}{1 + Q_c/\pi + (Q_s f_c)/(\pi f_s) + f_c \Delta}. \quad (1)$$

Here we have to note that the differential operator of the PID feedback circuit can partially compensate the phase delays. The feedback bandwidth is not determined only by Eq. (1), but also by the sample height ( $h$ ), the free oscillation amplitude ( $A_0$ ) of the cantilever, and the set-point ( $rA_0$ ) [10]. This is because the cantilever tip end tends to detach completely from the sample surface when scanning over a downhill, and its tendency is affected by these factors. Once detached, the tip end cannot re-land on the surface quickly (like 'parachuting'), because the

error signal is saturated at  $(1-r)A_0$ . The time required for re-landing is roughly proportional to  $\kappa \equiv h/(1-r)A_0$ . Therefore, the feedback bandwidth is also a function of  $\kappa$ . Although it is difficult to obtain an analytical expression for the function theoretically, we can obtain a quantitative expression experimentally [11]. The frame acquisition time ( $T$ ) is determined by the feedback bandwidth ( $f$ ), the scan size ( $L$ ), the number of scan lines ( $N$ ), and the apparent sample size ( $\lambda$ ), as shown below.

$$T = \frac{2NL}{\lambda f}. \quad (2)$$

## III. THE FIRST GENERATION OF HIGH-SPEED AFM

Let us look over the tapping-mode AFM system (Fig. 1) to find what we have to do to achieve a high imaging rate. The sample stage scanner, especially the  $z$ -scanner, should move very quickly without unwanted vibrations. The cantilever's resonant frequency should be very high so that it responds to the tip-sample interaction fast enough and the amplitude reading shortens. In addition, its spring constant should be minute. The dimensions of such cantilevers have to be very small. Therefore, the optical system for detecting the cantilever deflection should be compatible with such small cantilevers. The split photosensor should have a wide bandwidth, and the RMS-to-DC converter should quickly output the rms signal. The PID feedback circuit should operate quickly; in addition, the piezo drive amplifiers should have a wide bandwidth and should be able to produce a large current. The data acquisition system has to work very fast. As surveyed above, we have to optimize many devices to produce a high-speed AFM. For about 5 years prior to 2001, we developed all the devices and constructed a high-speed AFM capable of capturing one image (scan size, 250 nm; scan lines, 100) within 80 ms [6, 7]. Below, we briefly describe key devices that mainly contributed to the achievement of the high imaging rate.

**Sample stage scanner:** The device most difficult to develop was the sample stage scanner. We used stack-piezo actuators with the resonant frequency of 260 kHz in free oscillation and with the maximum displacement of  $4.5 \mu\text{m}$ . Three actuators were aligned perpendicularly to each other; the  $y$ -piezo displaces a base where the  $x$ -piezo is mounted, and the  $x$ -scanner displaces a base where the  $z$ -scanner is mounted. To reduce vibrations, the latter base was clamped tightly between two ball-guide stages. However, this clamping was not sufficient to minimize vibrations. Quick displacements of the  $z$ -piezo exerted impulsive forces on the base, causing vibrations of the base, and in turn vibrating the  $z$ -piezo itself. Thus, an additional  $z$ -piezo was attached to the opposite side of the base. The impulsive forces were counteracted by the simultaneous displacements of the two  $z$ -piezo actuators of the same length, in the counter direction. This counterbalance method was very effective in minimizing vibrations. The  $z$ -scanner had a nearly constant gain up to 60 kHz [6, 7].

**Small cantilevers:** Olympus made small cantilevers without tips from silicon nitride [6]. The dimensions were

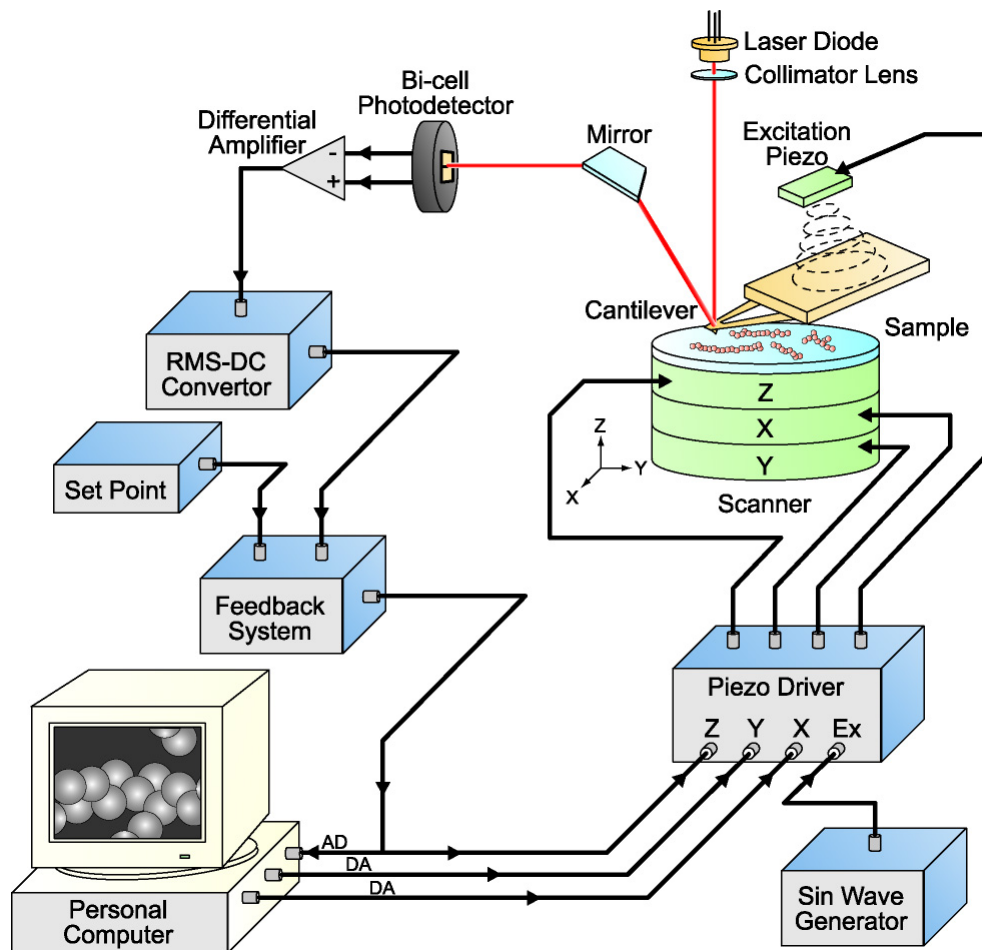


FIG. 1: Schematic presentation of the tapping-mode AFM system.

140 nm thick, 2  $\mu\text{m}$  wide, and 9  $\mu\text{m}$  long. The resonant frequencies were around 1.5 MHz in air and about 600 kHz in water, and the spring constant was about 150 pN/nm. The tips were grown by electron-beam deposition. As indicated in Eq. (1), the resonant frequency of the cantilever determines the upper limit of the feedback bandwidth to be  $600/8 = 75$  kHz.

**Amplitude-to-DC converter:** Conventional RMS-to-DC converters require at least a few numbers of waves of the input signal to output an accurate rms value. To increase the conversion rate, we developed an amplitude-to-DC converter using two sample/hold (S/H) circuits [6]. The peak and bottom voltages of the every input sinusoidal wave were held by the S/Hs, and their difference generated the amplitude signal. Therefore, the amplitude signal is renewed at every half cycle of the input signal.

By assembling these devices and other devices, we constructed a high-speed AFM mounted on an inverted type of optical microscope. Using this AFM, we succeeded in capturing myosin V molecules moving in solution on video at 80 ms/frame [6]. This was the first anyone has viewed a rapidly moving protein in solution with nanometer resolution.

#### IV. SECOND GENERATION OF HIGH-SPEED AFM

We later noticed that our high-speed AFM could not capture fragile samples such as microtubules without disassembling them [8]; still less is it possible to capture weakly interacting protein molecules such as actin-myosin V in the presence of ATP, without disturbing their interaction. The large tip-sample interaction seemed due to an insufficient feedback bandwidth and a too-strong tapping force. Therefore, in 2002 we began making further improvements to the small cantilevers, the scanner, and the feedback control.

**Smaller cantilevers:** Smaller cantilevers (Fig. 2) with a resonant frequency higher than the previous version were developed to enhance the feedback bandwidth [12]. The dimensions are 7  $\mu\text{m}$  long, 2  $\mu\text{m}$  wide, and 90 nm thick. The resonant frequencies are about 2.4 MHz in air and about 1.2 MHz in water, and the spring constant is about 200 pN/nm. Although the cantilevers have bird-beak like tips, their apex is not sharp enough. Therefore, EBD tips were grown on the bird-beak like tips.

**Dynamic PID controller:** To reduce the tapping force, we needed small cantilevers with a smaller spring constant. However, it was very difficult to make it compatible with the high resonant frequency. The other way to reduce the tapping force was to adjust the set-point of

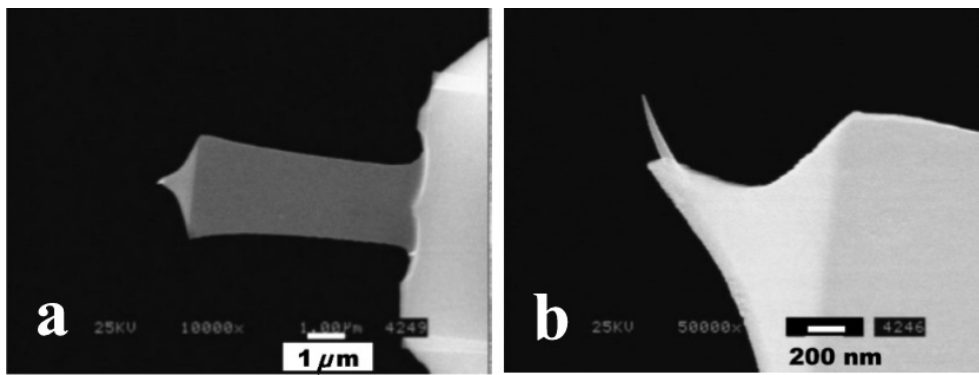


FIG. 2: Electron micrographs of the small cantilever chip with a birdbeak-like tip. (a) Top view; (b) a magnified image of the tip region. The protruding needle is an EBD tip.

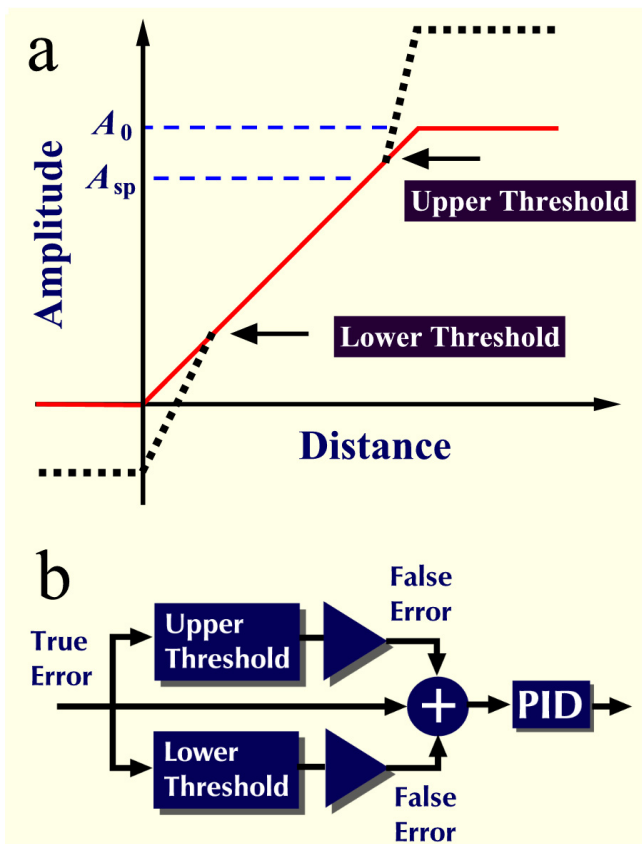


FIG. 3: Schematic presentation of the dynamic PID control technique. (a) Amplitude-distance curve (red line) and schematic outline of the dynamic PID control technique.  $A_0$  denotes the free oscillation amplitude of the cantilever, and  $A_{sp}$  denotes the set-point. The black dotted lines represent the false error signals added to the true error signals. (b) A diagram of the dynamic PID circuit.

the cantilever oscillation very close to its free oscillation amplitude. However, this adjustment results in a narrower feedback bandwidth, as mentioned in 'Theoretical Considerations'. With a large set-point, the parachuting period is prolonged because the PID circuit produces a small feedback signal that is proportional to the saturated-error signal, i.e.,  $(1 - r)A_0$  (where  $r$  is smaller

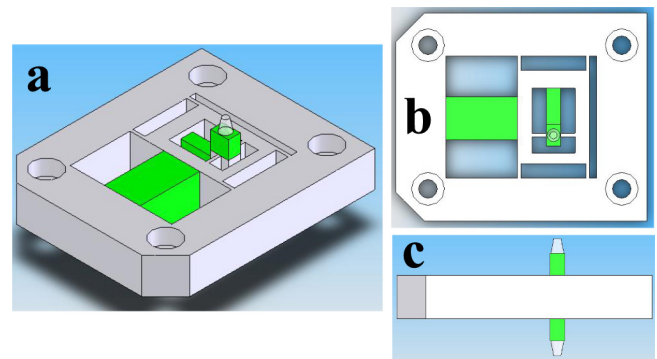


FIG. 4: Sketches of the high-speed scanner. (a) 3D view, (b) top view, and (c) side view. The green blocks are piezo actuators. A sample stage is attached on the top of the upper z-piezo actuator, and a dummy stage is attached on the top of the lower z-piezo actuator used for counterbalancing. The dimensions ( $W \times L \times H$ ) of the x-, y-, and z-actuators are  $2 \times 3 \times 5$ ,  $5 \times 5 \times 10$ , and  $2 \times 3 \times 3 \text{ mm}^3$ , respectively.

than 1, but very close to 1). To overcome this difficulty, we developed a new PID controller whose gain can automatically be changed depending on the error signal (Fig. 3) [8, 11]. A threshold level is set between  $rA_0$  and  $A_0$ . When the cantilever oscillation amplitude exceeds this threshold level, a false error signal is added to the true error signal. The resulting large error signal produces a large feedback signal, which reduces the parachuting period or prevents the cantilever tip from getting into the parachuting phase. This dramatically enhances the feedback bandwidth at a large set-point ( $r > 0.8$ ). A similar manipulation of the error signal is applicable also to the case where the cantilever oscillation amplitude becomes much smaller than the set-point. This is effective in preventing the cantilever tip from hitting the sample or the substratum too strongly.

**High-speed scanner:** We simplified the scanner design to reduce the number of resonant peaks as well as to increase the rigidity. Instead of the ball-guide stages, we employed a flexure stage (Fig. 4). In addition, we employed stack piezo actuators with a higher resonant frequency (470 kHz) for the z-scanner (the resonant frequency decreased to 150 kHz when they were embedded

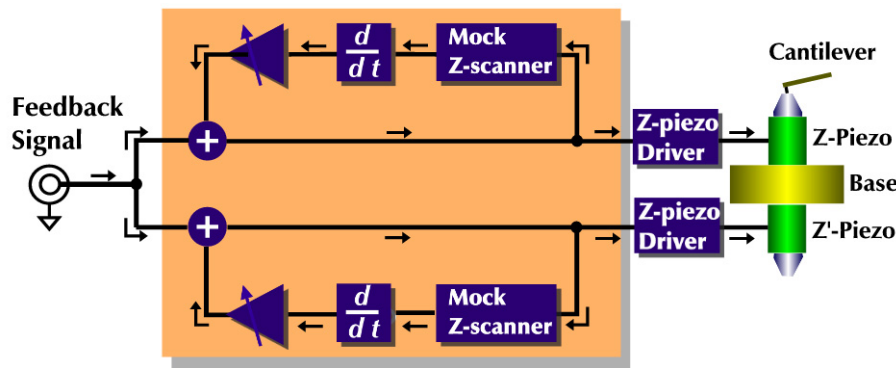


FIG. 5: A schematic of the active damping method. The feedback signal (output from the PID controller) is fed to the active Q-control circuit. The transfer function of the LCR circuits (mock z-scanners) is adjusted so as to become very similar to the z-scanner. The mock z-scanners can contain a number of LCR circuits corresponding to the multiple resonant components of the z-scanner.

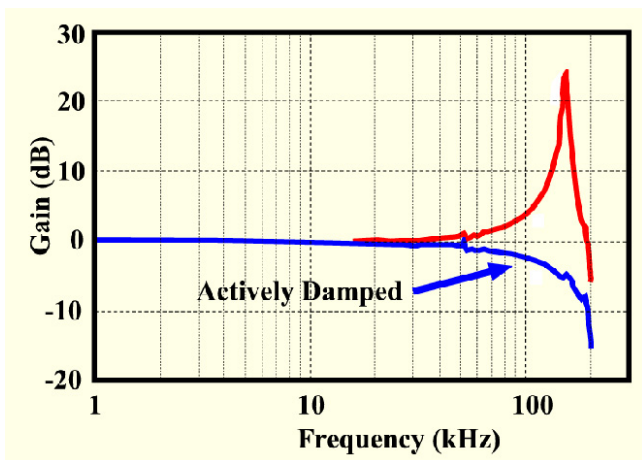


FIG. 6: Effect of the active damping on the resonance of the z-scanner. The curves are resonant gains with (blue line) and without (red line) operation of the active damping.

into the scanner). We again used the counterbalance method to minimize the structural resonance in the z-direction. Here, we made efforts to eliminate the resonance originating in the z-piezo actuator itself that could not be removed by the counterbalance [9]. In principle, it is possible to damp the resonant vibrations using a so-called active Q control of the vibrations. In this control, the displacement signal of the z-piezo actuator is differentiated, and its polarity is inverted. Then, its gain-controlled signal is added to the driving signal. This addition apparently increases the damping (or frictional) force, resulting in the reduction of the quality factor of the z-piezo resonance. However, in practice it is difficult to monitor the quick and unpredictable displacement of the z-piezo actuator during scanning. On the other hand, the dynamic behavior of the z-piezo is determined by its transfer function. We noticed that this transfer function was well approximated by a transfer function of a second-order low-pass filter that can be made simply by an LCR circuit. Therefore, it is possible to use, as a mock z-piezo, the second-order low-pass filter that is tuned to have the transfer function very similar to that of the z-

piezo (Fig. 5). This technique is also useful in eliminating the remaining small resonant vibrations originating in the scanner structure. As shown in Fig. 6, the resonant vibrations of the z-scanner were eliminated by this active damping method. Because the quality factor of the z-scanner's peak resonance was reduced from 18 to 0.5, its response speed was increased 36 times (the response time,  $\sim 1.1 \mu\text{s}$ ). Although the phase delay was pronounced by the active damping, it was suppressed by inverse transfer function compensation [9].

Because of the improvements mentioned above, the feedback bandwidth was enhanced up to 100~110 kHz under the conditions of  $r = 0.6 \sim 0.9$  and  $A_0/h = 2 \sim 5$ . Even with  $r = 0.95$  and  $A_0/h = 2 \sim 5$ , the feedback bandwidth was around 80 kHz [11]. This small dependence of the feedback bandwidth on the set-point (due mainly to the effect of the dynamic PID control) guarantees that imaging can be carried out with a weak tapping force. According to Eq. (2), the wide feedback bandwidth promises the imaging rate of  $\sim 50$  ms/frame under the conditions of  $N = 100$ ,  $L = 250$  nm, and  $\lambda = 10$  nm.

## V. BIOIMAGING

Here, we show some examples of the image data obtained by the high-speed AFM. However, these images were not obtained after completing the second generation of AFM, but most were obtained during this development. Therefore, the imaging rates used are mostly not the maximum rate that has now become available.

The first data show how small the tip-sample interaction force is. The interaction between actin filaments and myosin V in the presence of ATP is highly dynamic and hence very weak. Actin filaments move over a surface that is coated densely with myosin V molecules. This movement was successfully captured on video, without disturbing their weak interaction (Fig. 7a, Movie 1 in Electronic Appendix). The velocity of actin filament gliding was very similar to that observed by fluorescence video microscopy. To view the dynamic behavior of individual myosin V molecules when they are propelling actin filaments unidirectionally, the surface was sparsely coated with myosin

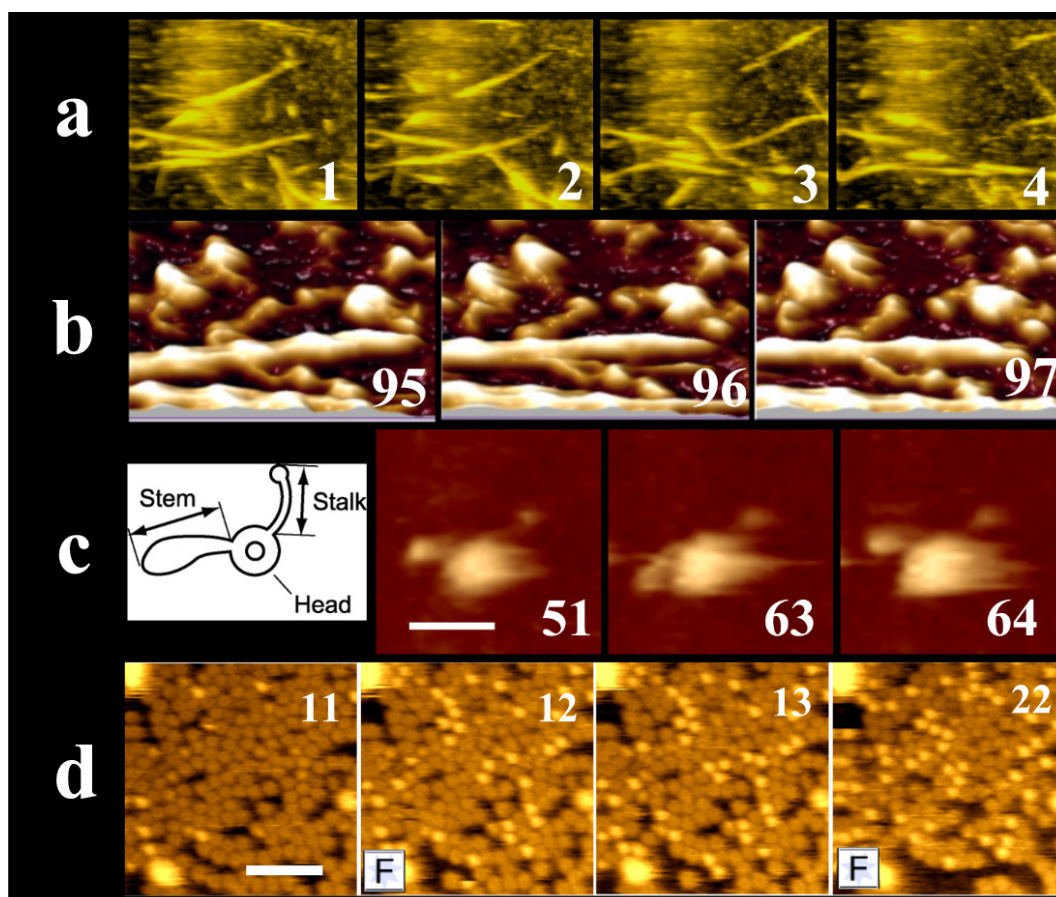


FIG. 7: Successive AFM images of various samples. The numbers attached indicate the frame numbers. Corresponding AFM movies can be viewed at Electronic Appendix. (a) Actin filaments that are sliding over the myosin V-coated mica surface in the presence of ATP. The scan range, 1  $\mu$ m; the scan speed, 1s/frame. (b) Myosin V that is propelling sliding movement of a short actin filament in the presence of ATP. The distance between the adjacent bumps of the actin filament is 36 nm. The frame rate is 160 ms/frame. (c) The left panel is a schematic drawing of dynein C. The stem stays mainly at the position as shown in the frame 51 and 64 (corresponding to the non-nucleotide-bound state), and occasionally moves to the position shown in the frame 63 (corresponding to the nucleotide-bound state). Scale bar, 30 nm. (d) GroES binding to GroEL just after ATP release by flash-photolysis of caged-ATP. UV flash light was applied shortly before the frames marked with 'F'. Scale bar, 100 nm.

V. A short actin filament whose entire length was within the imaging region was observed (Fig. 7b). This fortunate situation allowed us to identify which myosin V molecules were propelling the actin filament. Two myosin V molecules were interacting with the short actin filament, and only one of the two heads of each myosin V molecule was attached to the actin filament. The actin filament moved leftward in a stepwise manner (Movie 2 in Electronic Appendix); the step size was 36 nm, which corresponds to half of the long helical repeat of an actin filament. During the stepwise movement, the interacting heads did not seem to change their conformations much, which was not the behavior expected from the well-studied swinging-lever arm hypothesis in which a large swinging movement of myosin's neck domain is supposed to propel the actin filament [13].

Dynein C is a single-headed dynein. A stalk and a stem protrude from the ring-shaped head (Fig. 7c), and the stalk interacts with microtubules at the globular distal end. Electron micrographs of dynein C have revealed that the angle between the stalk and the stem differed between the apo state (no-nucleotide) and the ADP-Vi-

bound state [14]. The nucleotide-dependent change in the structure is hypothesized to drive microtubule movement. However, ADP-Vi is a non-natural substrate, and therefore it is not certain that such a change of angle really occurs during the ATPase cycle. High-speed AFM imaging of dynein C in the presence of ATP revealed that it did certainly occur. The stalk and the head seemed stationary, but the stem went back and forth between two positions (Fig. 7c, Movie 3 in Electronic Appendix). The stem-stalk angle changed between  $137^\circ$  and  $184^\circ$ ; the former angle corresponds to the apo state, while the latter was larger than that of the ADP-Vi-bound state ( $159^\circ$ ). The frequency of the change in angle approximately coincided with the ATPase rate. Therefore, it is very certain that the stem movement observed is driven by the ATPase reaction. This is the first time that a cyclic protein's conformational change has been captured on video in real time.

The UV-photolysis of caged ATP [14] was applied to the GroEL-GroES system [15]. GroEL is a chaperonin that assists its substrate polypeptides in folding into their functional 3D structures, and GroES is a co-chaperonin.

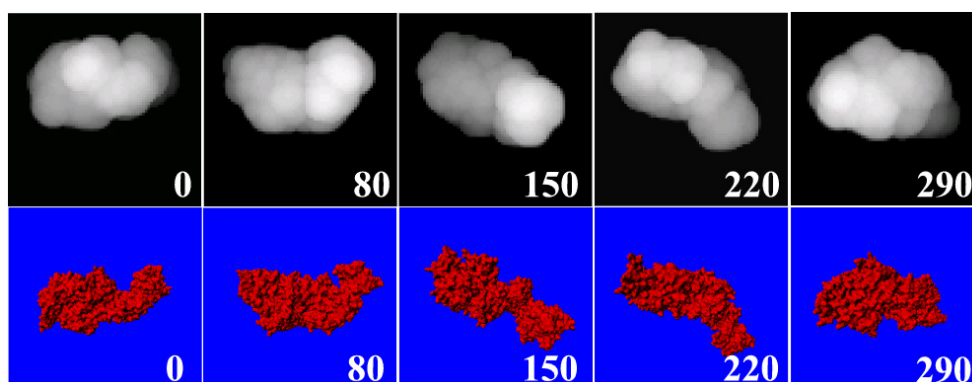


FIG. 8: Pseudo AFM images constructed from the atomic structure of myosin V subfragment-1. The pseudo AFM images are shown on the upper line, and their corresponding appearances of the atomic model viewed from the same angles are shown on the lower line. The atomic model is rotated around a horizontal axis, and the number attached to each panel indicates the rotation angle.

GroEL consists of two homo-heptameric rings that are stacked back-to-back, whereas GroES is a single homo-heptameric ring. GroES binds to GroEL only when GroEL is in the nucleotide-bound state. GroEL was attached to the mica surface with an end-up orientation, forming a highly packed single layer. The central channel of the GroEL ring was therefore visible. Before UV application, GroES was floating in the solution containing caged-ATP, and therefore not visible. High-frequency pulses of a UV laser light (355 nm) were applied within 5 ms while the  $y$ -return scanning was performed. Immediately after this, GroES attached to the top of GroEL, forming protrusions on the GroEL layer (Fig. 7d, Movie 4 in Electronic Appendix). Because the concentration of the ATP that was produced in the small UV-irradiated volume quickly fell due to diffusion, the second application of the UV pulses resulted in more protrusions.

The last image data of myosin V alone were obtained after completing the second generation of high-speed AFM. The frame rate reached about 50 ms/frame (Movie 5 in Electronic Appendix). With a higher rate, the scanner produced vibrations in  $z$ -direction because of the low resonant frequency of the  $x$ -scanner. We are now improving the  $x$ -scanner.

When dynamic behavior of a protein with a known atomic structure is captured on video, is it possible to understand the dynamic behavior in light of the atomic structure? When a protein does not have a unique shape at a few-nanometer resolution, it is difficult to understand from the video image which face of the molecule is imaged, which part is bending or twisting, and so on. As a first step for understanding these aspects, we have been trying to fit an AFM image of myosin V subfragment-1 on mica to its atomic structure. The fitting procedures are as follows. First, we obtain the surface coordinates of the atomic model. Next, considering the effect of the radius and the cone angle of the cantilever tip on the AFM image formation, we construct a library of many pseudo AFM images, looking at the atomic model from various angles (Fig. 8). We compare a top-view (2D profile) of an AFM image with those of the pseudo AFM images to choose a number of fit candidates. Then, we compare the 3D profile of the AFM image with those of the chosen candidates

to find the best-fit pseudo AFM image. The three candidates chosen by the 2D-profile fitting resemble to each other (the right upper panels of Fig. 9). The 3D-profile fitting gave the best score of fitting to the one shown in the column "1". This result seems reasonable, because myosin V subfragment-1 in the best-fit orientation has a cluster of positive charges on the backside, which must facilitate its binding to the negatively charged mica surface. In these procedures, we have not considered conformational changes of the protein. However, it is likely that the entire conformation does not change but the relative orientation between the domains does (thus, each domain conformation is rather unchanged). Therefore, to include a possible conformational change in the fitting procedures, we may have to divide an AFM image of a protein molecule into two or three domains and fit them separately. Of course, for this fitting to be successful, the high-resolution AFM images are required. If we have a rational way to distort the atomic model, it would become possible by using the fitting results to construct a dynamic atomic model that reflects the dynamic behavior of the protein recorded on the AFM video.

## VI. TOWARD THE NEXT GENERATION

Although third-generation AFM is not yet complete, here we briefly mention how we have been working toward the third generation of our high-speed AFM. To enhance the feedback bandwidth, it is important to increase the resonant frequency of the  $z$ -scanner, but available piezoactuators are limited. We estimate that the achievable maximum resonant frequency of a piezo-stage scanner will be limited to be about 300 kHz, only twice that of our  $z$ -scanner. Self-actuating cantilevers are an alternative to the piezo-stage scanner, but a cantilever with an integrated zinc oxide piezoactuator inevitably becomes too stiff. Driving a cantilever coated with a thin magnetic film directly by a magnetic field is also an alternative [16]. However, a magnetic-film coating sufficient for the cantilever to be driven reduces the resonant frequency of the cantilever. To drive a cantilever by a different means, we measured the cantilever deflec-

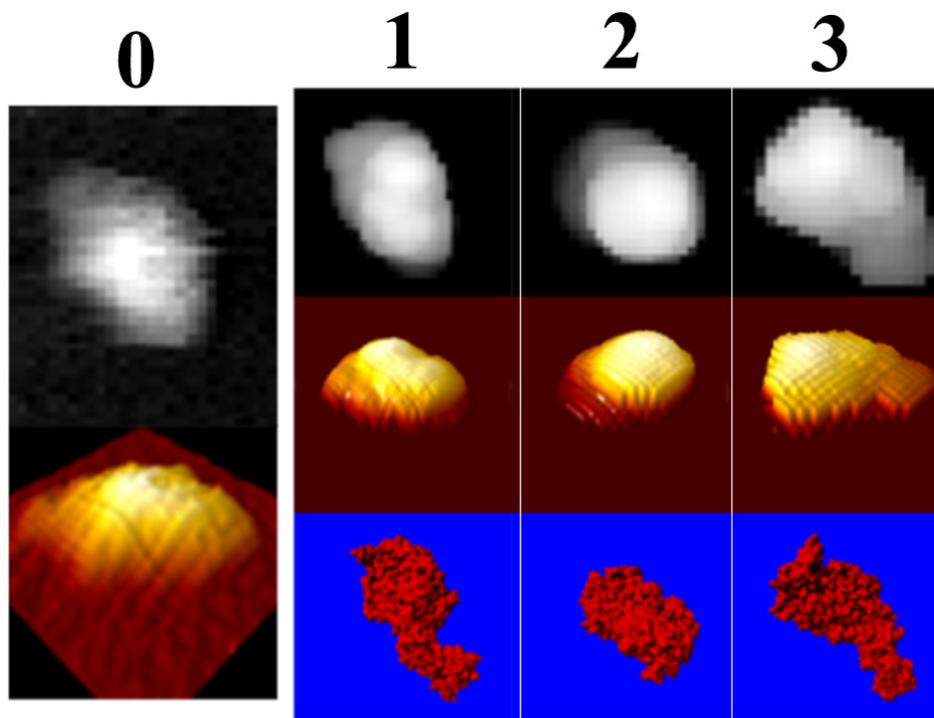


FIG. 9: Fitting of an AFM image of myosin V subfragment-1 to the pseudo AFM images. Column 0 shows a top view (upper panel) and a 3D view (lower panel) of the AFM image. Columns 1, 2, and 3 show pseudo AFM images (upper and middle lines) and corresponding appearances of the atomic model viewed from the three angles (lower line). These three give good scores on the fitting test of the 2D profiles. Column 1 gives the best score on the fitting test of the 3D profile.

tion caused by photo-thermal expansion of gold coated onto a  $\text{Si}_3\text{N}_4$  cantilever surface [17]. The sensitivity was about 10 nm/mW in aqueous solution when a 405-nm violet laser was used with our small cantilevers. Because of the slow heat-transmission process, the response time of the deflection was about 30  $\mu\text{s}$ . However, inverse transfer function compensation was apparently able to eliminate the slow heat-transmission process [17]. Because the maximum displacement of the cantilever driven by photo-thermal expansion is so far limited, and the "cantilever scanner" requires a large dynamic range of the deflection detection sensor (which reduces the sensor sensitivity), it is apparent that this technique has to be used together with the conventional piezo-stage scanner. Photo-thermal expansion can also be used to directly excite a cantilever at its resonant frequency [17, 18]. Unlike acoustic excitation, it does not have the "forest of peaks" effect. This superior attribute facilitates the active control of the cantilever to reduce  $Q$ , which enhances the response speed of the cantilever (and hence the feedback bandwidth).

Another device that we have been trying to include in the third generation of our high-speed AFM is a feed-forward controller [19]. Topographic differences between two adjacent line-scans are not large, as long as the sample is not moving rapidly. Therefore, line-by-line feed-forward control can lighten the feedback-control task; in other words, the dependence of the feedback bandwidth on  $\kappa$  (see Section "Theoretical Considerations") is reduced by the feed-forward control. Using stationary samples, we confirmed that a significant extension of the feedback bandwidth was achieved by the feed-forward control [18].

However, when the sample is moving quickly, the feed-forward control is expected to act occasionally in an undesirable direction. Yet, we have not noticed any ill effect that would be expected to result from such an undesirable action, even with rapidly moving samples. This may be due to a small time-difference (less than 1 ms) between two line-scans.

## VII. CONCLUSIONS

The second generation of our high-speed AFM has the capacity to dissect dynamic processes of individual protein molecules at work. The compatibility of the high scan rate and a skimming scan over fragile samples has been successfully achieved. The scan rate has reached a level where video-rate imaging is almost possible. The tip-sample interaction force is greatly reduced to a level where it does not disturb weak protein-protein interactions.

## Acknowledgments

This work was supported by CREST/JST, Special Coordination Funds for Promoting Science and Technology (Effective Promotion of Joint Research with Industry, Academia, and Government) from JST, and a Grant-in-Aid for Basic Research (S) from the Ministry of Education, Sports, Science, and Technology of Japan.

- 
- [1] P. K. Hansma, J. P. Cleveland, M. Radmacher, D. A. Walters, P. E. Hillner, M. Bezanilla, M. Fritz, D. Vie, H. G. Hansma, C. B. Prater, J. Massie, L. Fukunaga, J. Gurley, and V. Elings, *Appl. Phys. Lett.* **64**, 1738 (1994).
  - [2] M. B. Viani, T. E. Schäffer, A. Chand, M. Rief, H. E. Gaub, and P. K. Hansma, *J. Appl. Phys.* **86**, 2258 (1999).
  - [3] M. B. Viani, T. E. Schäffer, G. T. Paloczi, L. L. Pietrasanta, B. L. Smith, J. B. Thompson, M. Richter, M. Rief, H. E. Gaub, K. W. Plaxco, A. N. Cleland, H. G. Hansma, and P. K. Hansma, *Rev. Sci. Instrum.* **70**, 4300 (1999).
  - [4] S. R. Manalis, S. C. Minne, and C. F. Quate, *Appl. Phys. Lett.* **68**, 871 (1996).
  - [5] M. Lutwyche, C. Andreoli, G. Binnig, J. Brugger, U. Drechsler, W. Häberle, H. Rohrer, H. Rothuizen, P. Vettiger, G. Yaralioglu, and C. Quate, *Sensors and Actuators* **73**, 89 (1999).
  - [6] T. Ando, N. Kodera, E. Takai, D. Maruyama, K. Saito, and A. Toda, *Proc. Natl. Acad. Sci. USA* **98**, 12468 (2001).
  - [7] T. Ando, N. Kodera, D. Maruyama, E. Takai, K. Saito, and A. Toda, *Jpn. J. Appl. Phys.* **41**, 4851 (2002).
  - [8] T. Ando, N. Kodera, Y. Naito, T. Kinoshita, K. Furuta, and Y. Y. Toyoshima, *Chem. Phys. Chem.* **4**, 1196 (2003).
  - [9] N. Kodera, H. Yamashita, and T. Ando: *Rev. Sci. Instrum.* **76**, 053708 (2005).
  - [10] T. Sulchek, G. G. Yaralioglu, C. F. Quate, and S. C. Mine: *Rev. Sci. Instrum.* **73**, 2928 (2002).
  - [11] N. Kodera, and T. Ando (in preparation)
  - [12] M. Kitazawa, K. Shiotani, and A. Toda, *Jpn. J. Appl. Phys.* **42**, 4844 (2003).
  - [13] G. Tsiavaliaris, S. Fujita-Becker, and D. J. Manstein, *Nature* **427**, 558 (2004).
  - [14] S. R. Adams, and R. Y. Tsien, *Ann. Rev. Physiol.* **55**, 755 (1993).
  - [15] K. Braig, Z. Otwinowski, R. Hegde, D. C. Boisvert, A. Joachimiak, A. L. Horwich, and P. B. Sigler, *Nature* **371**, 578 (1994).
  - [16] W. Han, S. M. Lindsay, and T. Jing, *Appl. Phys. Lett.* **69**, 4111 (1996).
  - [17] T. Ando, T. Uchihashi, N. Kodera, A. Miyagi, R. Nakakita, H. Yamashita, and M. Sakashita, submitted to *Jpn. J. Appl. Phys.*
  - [18] T. Uchihashi, N. Kodera, H. Itoh, H. Yamashita, and T. Ando, submitted to *Jpn. J. Appl. Phys.*
  - [19] G. Schitter, F. Allgöwer, and A. Stemmer, *Nanotechnol.* **15**, 108 (2004).